Few layer graphene does not affect the function and the autophagic activity of primary lymphocytes

Diane Murera,[1] Sowmya Malaganahalli,[1] Cristina Martín,[1] Giacomo Reina,[1] Jean-Daniel Fauny,[1] Hélène Dumortier,[1] Ester Vázquez,[2,3] Alberto Bianco[1,]*

[1]University of Strasbourg, CNRS, Immunology, Immunopathology and Therapeutic Chemistry, UPR 3572, 67000 Strasbourg, France. E-mail: a.bianco@ibmc-cnrs.unistra.fr
[2]Instituto Regional de Investigación Científica Aplicada (IRICA), Universidad de Castilla-La Mancha, Avda Camilo Jose Cela, 13071 Ciudad Real, Spain.
[3]Departamento de Química Orgánica, Facultad de Ciencias y Tecnologías Químicas, Universidad de Castilla-La Mancha, 13071 Ciudad Real, Spain.

Keywords: Graphene, immune cells, activation, autophagy, reactive oxygen species, mitochondria

Abstract

Carbon-based nanomaterials represent a new tool in future medical applications. Thus, focusing on the evaluation of the degree of their safety has been growing in the last years. In this study we were particularly interested in understanding the impact of few layer graphene (FLG) on primary murine lymphocytes. These B and T cells, that are the second, but specialized, line of defense of the immune system, rely on various mechanisms to ensure their efficient function and maintenance. One of these mechanisms is autophagy that can be triggered by various nanomaterials in some types of cells. For these reasons, we were interested to evaluate the way FLG could affect this process in lymphocytes. Our results point out that FLG does neither impact the viability and activation of T and B cells, nor their autophagic activity. Using confocal microscopy, we were also able to see that FLG does not appear to cause any membrane damages and that does not penetrate inside of these cells. Overall, our data do not show any impact of this material on lymphocyte homeostasis, which is one more argument in favor of the continuation of studies investigating the potential of FLG for therapeutic applications.

1. Introduction

Graphene-based materials (GBMs) such as graphene or few layer graphene (FLG) harbor a myriad of properties that make them suitable for various tasks ranging from electronics, photonics to biomedical applications.[1,2] These 2-dimensional sheets, organized in a honey-comb like structure, are excellent charge carriers with a high mechanical strength. They can be used for reinforcing composites and as efficient sensors.[3–5] These properties make also graphene a promising and valuable candidate in nanomedicine with a high potential in diagnosis and in therapy.[6,7] Indeed, graphene with its elasticity and strength, could be on one hand an excellent alternative to existing metallic or silicone implants, but also a unique material to design biosensors, drug and/or gene delivery systems.[8]

To explore the potential of FLG, especially in a biomedical context, it is of high importance to first investigate the risk to induce cytotoxic effects and/or to disturb specific intracellular processes. Evaluating the safety of nanomateriale (NMs) is indeed one of the major concerns in the nano-field.[2] The first step towards this goal is to start the inquiry at the cellular level. The interactions of GBMs with cells, as mostly demonstrated with graphene oxide (GO), the oxidized form of graphene, have been shown to be highly dependent on the cell type but also to trigger various mechanisms potentially leading to cell death.[9,10] One recurrent observation, in cells interacting with GBMs, is the production of significant amounts of reactive oxygen species (ROS) leading thus to oxidative stress.[2,6,9] Another mechanism that has been associated to these materials is macroautophagy. This process, aimed to maintain cellular homeostasis, can also be activated by stress signals, such as ROS. Macroautophagy is a lysosomal degradation pathway mainly targeting cytoplasmic content such as aggregated proteins and damaged organelles. It is characterized by a multi-step process leading to the formation of double membrane vesicles called autophagosomes. Their subsequent fusion with lysosomes completes the process and results in the breakdown and turnover of the captured material.[10] Macroautophagy, more commonly referred to as autophagy, is not solely a pro-survival mechanism but has paradoxically also been associated to apoptosis in cases of either the blockade or an overactivation of the process.[11] Some NM have indeed been reported to be able to modulate autophagy in various ways.[12] GO for instance appears to increase autophagy in macrophages, while carbon nanotubes induce a blockade of the autophagic flux as demonstrated in human umbilical vein endothelial cells and in macrophages.[13–15] Autophagy is also tightly linked to immune responses such as inflammatory responses, antigen presentation, pathogen clearance or lymphocyte homeostasis.[16] Since the immune system represents the first line of defense against any foreign element, we were interested in exploring the possible influence of FLG on autophagic functions of primary immune cells and in particular murine lymphocytes.

Only few and quite recent studies have been focused on understanding the impact of graphene or FLG on mammalian cells, and most of them were investigating the impact of graphene on cell lines with the exception of a study by Russier *et al.* that showed that FLG was able to selectively kill pathogenic monocytes from myelomonocytic leukemia patients.[17–19] However, to the best of our knowledge, no study has been looking into the impact of FLG on primary lymphocytes and on their autophagic activity. As these cells are key players in adaptive immunity, it appears essential to understand how FLG could interact with them.

2. Materials and methods

2.1. Graphene preparation and characterization

Few-layer graphene (FLG) was prepared by ball-milling treatment, according to previous published procedures.[20,21] In general, a mixture of graphite and melamine (1,3,5-Triazine-2,4,6-triamine) (7.5 mg of SP-1 graphite powder, purchased from Bay Carbon, Inc., and 22.5 mg of melamine purchased from Sigma-Aldrich) was ball milled at 100 rpm for 30 min using a Retsch PM 100 planetary mill under air. The resulting solid mixture was dispersed in 20 mL of water and sonicated for 1 min to produce a dark suspension. Melamine is afterwards eliminated by dialysis. Some precipitate, consisting in poorly exfoliated graphene, was removed from the liquid fraction after stabilization for 5 days. The final FLG water dispersions were lyophilized and the final graphene powder was thoroughly characterized.

Quantitative elemental analysis on FLG was performed with a LECO CHNS-932 elemental analyzer. FLG was also studied by TEM. A stable dispersions of the nanomaterial was drop-cast on a nickel grid (3.00 mm, 200 mesh) and dried under vacuum. The sample was studied by high-resolution transmission electron microscopy (HRTEM) JEOL 2100 at an accelerating voltage of 200 kV. Lateral dimension distribution was calculated by using Fiji-win64 software. In addition, the dispersion of FLG was drop-cast onto a Si wafer and dried on a hot plate in order to study the Raman spectrum. At least 20 Raman measurements were collected

in different locations using a Renishaw inVia Reflex Microscope at 532 nm with a 100× objective and an incident power of 1% (1 $mW\mu m^{-2}$).

2.2. Dispersibility study

FLG was resuspended in culture medium RPMI 1640 (Lonza BioWhittaker, Levallois, France) supplemented with 10% FBS at a working concentration of 100 mg mL^{-1} in a homemade chambered coverglass. Fluorescein sodium salt (Fluka Chemika, Buchs Switzerland, 46960) was added and the sample was analyzed by live imaging at 0 h, 2 h and 24 h, using an inverter Axio Observer Z1 micrsocope (Zeiss, Oberkochen, Germany, 100× objective). The count of the aggregates was achieved using the ImageJ software (National Institute for Health, Washington, DC, USA) on three images for each time point.

2.3. Animal experiments

BALB/c mice were used when they were between 8 and 13 weeks old. They were housed in the IBMC animal facility (agreement number G67-482-2). All experiments were carried out in conformity with the 2010/63/UE European animal bioethics legislation (French decree #2013-118 - 1st February 2013) and were approved by the Regional Ethics Committee of Strasbourg (CREMEAS) and by the French Ministry of Higher Education and Research (APAFIS#3280-2015121815099907 v2).

2.4. Cell isolation and cell culture

T and B lymphocytes were isolated from the spleens of BALB/c mice (8-13 weeks old) using the Dynabeads untouched mouse T cell isolation kit (Thermo Fisher Scientific, Illkirch, France, 11413D) or the Miltenyi Pan B isolation kit II (Miltenyi Biotec, Bergisch-Gladbach, Germany, 130-090-862), respectively. 15-20×10^6 T cells and 20-35×10^6 B cells were isolated form the spleen of a mouse. The efficiency of isolation was determined by flow cytometry by specific B and T cell staining with a purity nearing 95%. The cells (2.5×10^6) were then stimulated with phorbol 12-myristate 13-acetate (abbreviated P, 50 ng mL^{-1}, Sigma, P8139)

and ionomycin (abbreviated Iono or I, 1 µM, Sigma, I0634) or with purified NA/LE hamster anti-mouse CD3 (5 µg mL^{-1}, precoated, BD Biosciences, clone 145-2C11, 553057) and purified NA/LE hamster anti-mouse CD28 (5 µg mL^{-1}, BD Biosciences, clone 37.51, 553294) for T cells and lipopolysaccharide (LPS, 5 µg mL^{-1}, from *Escherichia* coli O111:B4, Sigma, L2630) for B cells. FLG was added at various concentrations either immediately or 2 h after the different activation parameters when indicated. Cells were incubated for 24 h in a 24 well plate at 37°C, 5% CO_2 in RPMI 1640 medium (Lonza BioWhittaker) supplemented with 10% FBS, 10 µg mL^{-1} gentamycin (Lonza BioWhittaker), 10 mM HEPES (Lonza BioWhittaker) and 0.05 mM β-mercaptoethanol (Lonza BioWhittaker).

2.5. Flow cytometry analysis

The cells (5×10^5) cells were stained with the following antibodies purchased from BD Bioscience (Le Pont-De-Claix, France): phycoerythrin (PE)-labeled anti-mouse CD86 (clone GLI, 553692), Peridinin-chlorophyll proteins (PerCp)-Cyanin 5.5-labeled anti-mouse CD19 (clone ID3, 551001), PE-labelled anti-mouse CD62L (clone MEL-14, 553151), allophycocyanin (APC)-labeled anti-mouse CD44 (clone IM7, 559250) and fluorescein isothyocyanate (FITC)-labeled annexin-V (560931). The fixable viability dye (FVD) efluor 780 (65-0865-14), the mitochondrial superoxide indicator MitoSOX™ Red (M36008), MitoTracker™ Green FM (M7514) and MitoTracker Deep Red (M22426) were purchased from Thermo Fisher Scientific (Fisher Scientific, Pittsburgh, PA, USA,).

2.6. Western Blot

For western-blotting, 2×10^6 cells were collected after 24 h incubation. When indicated protease inhibitors pepstatin A and E64D (5 µg mL^{-1}, Sigma-Aldrich; P5318 and E8640) were added 4 h prior to the end of the culture. The cells were then lyzed using Laemmli buffer (125 mM Tris-HCl, pH 6.8; 2% (w/v) sodium dodecyl sulphate (SDS); 10% (v/v) glycerol; 5% (v/v) β-mercaptoethanol) for total protein extraction. The proteins were separated by electrophoresis on a 4-20% polyacrylamide pre-cast gel (Bio-Rad, Hercules, CA, USA)

before being transferred on a nitrocellulose membrane (Bio-Rad), PBS supplemented with 5% (w/v) non-fat dry milk (Bio-Rad, ref) and 0.1% Tween-20 was used for blocking the membranes for 1 h. Monoclonal anti-LC3 antibodies (1 µg mL^{-1}) or horse radish peroxidase (HRP) coupled anti-Actin β (0.1 µg mL^{-1}, Santa Cruz Biotechnology, Heidelberg, Germany, clone C4, sc-47778 HRP) were incubated for 1h at room temperature (RT). For LC3 detection, a secondary anti-mouse IgG antibody coupled to HRP (Southern Biotech, Birmingham, AL, USA; 1030-05) was used. The membrane was then incubated for 2 min with the HRP substrates for chemiluminescence (Immobilon Western, Merck Millipore, Darmstadt, Germany; WBKLS0500). The resulting signal was visualized on photographic films and quantified by measuring the density of the bands using the ImageJ software.

2.7. Immunofluorescence staining and acquisitions

After 24 h incubation, ~500.000 T or B lymphocytes were transferred in a poly-L-lysine (Sigma-Aldrich, P8920-100ML) coated 8 chamber BD Falcon culture slide (Corning Life Sciences DL, Tewksbury, MA, USA, 08-774-26). After 1 h incubation at 37°C, 5% CO_2, to favor adherence, the cells were washed in Tris-buffered saline (TBS) pH=7,4 and subsequently fixed in 2% (v/v) paraformaldehyde for 30 min at room-temperature (RT). Then the cells were washed again, before incubation in a permeabilization solution (0.05% (v/v) Triton, 2% v/v fetal bovine serum (FBS) in TBS, for 30 min at RT. The following primary antibodies were incubated with the cells over night at 4°C in TBS supplemented with 1% (v/v) FBS: anti-LC3 (5 µg mL^{-1}, MBL, rabbit anti-mouse polyclonal antibody, NB100-2220), anti-Lamp2 (1 µg mL^{-1}, Santa Cruz, goat anti-mouse polyclonal, sc-8100), biotinylated anti-TCRb (2.5 µg mL^{-1}, Biolegend, hamster anti-mouse IgG2, clone DO-11.10, 109204), biotinylated anti-I-A/I-E (2.5 µg mL^{-1}, BD Pharmingen, rat anti-mouse IgG2a, clone 2G9, 553622). After washing with TBS, the cells were incubated for 1 h at RT with the respective secondary stainings: an Alexa-488 coupled goat anti-rabbit antibody (2 µg mL^{-1}, Molecular Probes A11034), a donkey anti-goat biotine antibody (Jackson, 705-065-147) and a

streptavidine-Alexa-546 (2 µg mL^{-1}, Molecular Probes, S11225). At the same time DAPI (4′,6-diamidino-2-phenylindole dihydrochloride) was added to stain DNA (50 µg mL^{-1}, D1306, Molecular Probes). After mounting the slides in Fluoromount-G fluorescence mounting medium (Thermo Fisher Scientific, 00-4958-02), they were observed under a confocal microscope. Pictures were acquired either on a spinning disk microscope (Zeiss Axio Observer Z1 with a Yokogawa CSU X1 confocal head) or on a LSM780 microscope (Zeiss Axio Observer Z1 with a LSM780 confocal head). The pictures shown in Figure 6 were acquired on a LSM780 microscope (Zeiss Axio Observer Z1 with a LSM780 confocal head). Each fluorophore was acquired separately using 405/488/561 and 633 nm lasers to get their spectra. The samples stained with all fluorophores were acquired using the spectra such obtained and fluorophores were separated spectrally using the unmixing module of Zen acquisition software of Zeiss Company. The pictures in Figures S2 and S3, and the corresponding videos, were acquired on a spinning disk microscope (Zeiss Axio Observer Z1 with a Yokogawa CSU X1 confocal head). The images were acquired sequentially using a Plan-Apochromat 100× objective NA1.4. DAPI was acquired using a 405 nm laser and a BP450/50 emission filter. LC3 was acquired using a 488 nm laser and a BP525/50 emission filter. TCRb and MHCII where acquired using a 561 nm laser and a BP629/62 emission filter. QD where acquired using a 488 nm laser and a BP690/50 emission filter. The z-stack shown in Video S1 was acquired on a Zeiss Axio Observer Z1 in widefield fluorescence microscopy with a Plan-Apochromat 100× objective. Pictures were acquired using the Set 44 filter cube of Zeiss company. The images were analyzed using the ImageJ software.

2.8. FLG-QD preparation

QD have been prepared as described in the literature.[22] $InCl_3$ (88.4 mg, 0.4 mmol) was added to $AgNO_3$ (17 mg, 0.1 mmol) in a 100 mL round bottom flask. Subsequently, 190 µL of oleic acid (0.6 mmol), 720 µL of dodecylthiol (3 mmol) and 8 mL of octadecene were added under vigorous stirring (420 rpm). The dispersion was flushed with argon for 15 min. Subsequently

the temperature was risen and kept at 60°C for 15 min, then at 95°C for 15 min, and 110°C for other 15 min until dissolution of indium and silver salts. After, 9.6 mg (0.3 mmol) of S dissolved in 4 mL of oleylamine were rapidly added with a syringe. Immediately, the solution turned from pale pink to dark pink. After 15 min, 70.5 mg (0.5 mmol) of $ZnCl_2$ dissolved in 3 mL of oleylamine and 2 mL of 1-octadecene were added and the temperature was increased to 150°C and kept for other 15 min. Then, the reaction was chilled with an ice bath and the crude compound was washed by 6 cycles of washing three times using ethanol and three times using acetone as anti-solvent. Finally, the QDs were dispersed in 20 mL of CH_2Cl_2 and stored at 4°C (concentration 2 mg mL^{-1}). Concentration was calculated evaporating and weighing the solid of a known volume of solution.

Coupling of FLG with QDs has been recently reproted by our group.[23] Briefly, 10 µL (2 mg mL^{-1} CH_2Cl_2) of QDs were added to 100 µL (100 µg mL^{-1}) aqueos dispersion of FLG. The biphasic solution have been sonicated at 40°C in a water bath for 10-15 min. As the organic phase evaporated unreacted QD have been separed via decantation, while the FLG-QD have been purified via centrifugation/washing several times with distilled water.

2.9. Statistical analysis

Based on the number of experiments and the number of conditions in each cellular test, a one-way ANOVA Tukey test was applied in order to evaluate the statistical significance.

3. Results and discussion

3.1. FLG dispersion in cell culture media

The main issue to overcome when working with graphene, is its poor dispersibility in water or in culture media. This is one of the reasons why so far, graphene oxide, was favored in most studies investigating the impact of graphene materials in biological systems and their potential use in biomedical applications[24]. However, in the last years, several exfoliation methods, aiming to overcome this difficulty, have been developed. The FLG used for this

study was obtained by mechanochemical exfoliation using a ball milling technique in the presence of melamine as the exfoliating agent. Briefly, a mixture of graphite and melamine was ball milled at 100 rpm for 30 min under air. The resulting solid mixture was dispersed in water and briefly sonicated to produce a dark suspension. Melamine was then eliminated by dialysis. Some precipitate, consisting in poorly exfoliated graphite, was removed from the liquid fraction after stabilization for 5 days.[20,21] The final FLG water dispersions were lyophilized and the final graphene powder was thoroughly characterized (Figure S1). The advantage of this graphene lies in the fact that it can be lyophilized and then easily resuspended in culture media. Transmission electron microscopy (TEM) analysis revealed a lateral size distribution of FLG ranging from 100 nm to 1600 nm (Figure S1A). Raman average spectrum of FLG is composed by the typical graphene Raman bands: G peak, D peak and 2D band, which are centered at ~ 1580 cm^{-1}, ~ 1350 cm^{-1} and ~ 2680 cm^{-1}, respectively (Figure S1C). A I_D/I_G ratio of 0.28 and the full-width at half maximum (FWHM) of 2D band of 65.54 cm^{-1} confirmed the few layer nature of the graphene sample.[20] The elemental analysis of FLG showed that the sample is mostly composed of carbon (Figure S1D), and the melamine traces resulted in maximum 0.93 ppm, as calulated from the powder dispersion at 0.1 mg mL^{-1}. We further investigated the amount and size of the possible aggregates formed in the culture medium over time by confocal microscopy, in order to study in a deeper way the material availability for the cells. By exploiting a property of graphene, namely its capacity to quench fluorescence, we resuspended the lyophilized FLG at a concentration of 100 µg mL^{-1} in fetal bovine serum (FBS) supplemented RPMI culture medium, in the presence of fluorescein. For this set of experiments, we used a 2 mL test vial capped with a cover slip on the bottom and filled with one ml of 0.1 mg mL^{-1} FLG dispersion. The images, taken on a widefield microscope at three different time points, were recorded in proximity to the cover slip where sedimentation would occur. As expected, due to the sedimentation process, the number of FLG aggregates visible in the vial bottom increased during time

(Figure 1A). Lateral size of the agglomerates was measured using the ImageJ software and analyzed as reported in Figure 1B and 1C. At the beginning, the sediment is composed by 31% of aggregates with lateral size ≥ 7 μm meanwile the composition of small aggregates of 5, 3 and 1 μm is 15, 23 and 31%, respectively. After two hours, the contribution of large big agglomerates is reduced to 20% while more than half of the population (51%) is composed by small aggregates (≤ 1 μm). After 24 h, the sediment was composed in majority of small agglomerates (≤ 1 μm 58%) while the contribution of larger aggregates (> 7 μm) is reduced to 6%. This latter tendency can be explained considering that the sedimentation velocity is strictly dependent on the particle size. For this reason, at the beginning the sediment is composed by a more prominent part of large aggregates. Subsequently FLG sheets in suspension tend to interact forming small aggregates that slowly precipitate. However, the movie obtained from different focal planes on the widefield microscope (See Supplementary Video S1) after 24 h confirmed that most of the small FLG aggregates are still in suspension. We would like to underline that the individual FLG nanosheets cannot be visualized by this technique. Besides, the observed micro-flakes can be deposited closely to or attached on the cell membrane and so they could induce direct stimulations to the cells through the physical contact.[25] Overall, this analysis was necessary to estimate the availability of FLG to the cells during the incubation. It appears indeed that at early time points, the material is mostly in suspension and can interact with cells that are also in suspension, as it is the case of the lymphocytes studied here.

3.2. Impact of FLG on lymphocyte viability and activation

The first step to understand the impact of FLG on lymphocyte function, was to evaluate its influence on their viability and activation. For this purpose, we incubated B or T lymphocytes isolated from spleens of BALB/c mice, for 24 h with a low (10 μg mL^{-1}) and a high (100 μg mL^{-1}) concentration of FLG alone or with FLG after pre-activating the cells, using either phorbol 12- myristate 13-acetate and ionomycin (P/I) or anti-CD3 and anti CD28

agonist antibodies for T cells and lipopolysaccheride (LPS) for B cells. Initially, we performed a dose response analysis using concentrations of 1, 10, 25, 50 and 100 µg mL^{-1}. As the results did not show any significant effect in the cellular tests, except on B cell activation at 100 µg mL^{-1} (data not shown), we considered the latter as the highest dose. However, to ensure that we did not miss events that might occur at low concentrations, we also used a dose 10 times lower in all experiments. The viability was assessed by flow cytometry using the fixable viability dye (FVD) and annexin V. FVD is a dye that crosses the membranes of dead cells and react with free amines in the cytoplasm, while annexin V detects apoptotic cells by binding phosphatidylserines. The gating strategy is shown in Figure 2A. FVD and annexin V negative subsets represent the percentage of live cells. As evidenced by these results, FLG seems to have no specific impact on the viability of the lymphocytes as the percentages of live cells remain about 60% with or without FLG (Figure 2B and 2C). The pre-activation improves the viability mainly in B lymphocytes without however being hampered neither by the low nor the high concentration of FLG. We then wanted to see whether FLG could play a role in the activation of these cells by measuring the expression of activation markers such as CD62L and CD44 for T cells and CD86 for B cells, respectively (Figure 2D). We did not see any difference in T lymphocyte activation even when the cells were pre-activated pharmacologically (P/I) or with agonist antibodies (anti-CD3/CD28) (Figure 2E). These results are in agreement with the study by Russier *et al*. in which the authors evaluated the impact of FLG on human peripheral blood mononuclear cells. In fact their screening on different human immune cell populations did not reveal any FLG mediated toxicity nor activation of T cells.[19] Similar observations were made on natural killer cells, on dendritic cells and on B cells. The observed effect was strictly restricted to monocytes. In the present study however, we noticed a dose dependent increase of the expression of the activation marker CD86 in the presence of graphene on B cells, with an increase of ~9% between the untreated condition and the low dose FLG and of ~20% with the high dose. With the P/I or

LPS stimulation, these differences were abolished (Figure 2F), potentially suggesting that at this time point we have reached the maximum activation threshold that cannot be further boosted, even in presence of FLG. Often in the literature we can see differences when various graphene materials are investigated, but in our conditions the material used was the same. Thus, the discrepancies with Russier *et al.* could be due to differences in the species (human *vs* mouse) but more likely to differences in the immunological compartments of interest in the two studies (peripheral blood *vs* spleen). Even though cross-species comparisons have been shown to vary between mouse and human, those are mainly at the developmental rather than the activation level.[19] However, in terms of B cell subsets, they can change depending on the compartments studied, with a higher proportion of mature B cells and some transitional 1 (T1) B cells in the periphery, while the spleen is populated by mature, T1 and T2 B cell subsets. In this context, we studied the effect of FLG on isolated B cells rather than on total PBMCs, composed of many different immune cells. Thus another hypothesis could be that we have a cumulative effect that might have passed unnoticed in a heterogenous immune cell population.

3.3. Study of lymphocyte autophagic function in the presence of FLG

Analyzing the results on cell viability and activation, we hypothesized that other mechanisms essential for lymphocyte homeostasis could be affected by FLG. As mentioned previously, autophagy is a major player in lymphocyte function. Thus, we decided to investigate if this process could potentially be modulated by graphene as well. For this purpose, we used the Western-blot technique for the detection of the membrane bound LC3-II protein, resulting from the conjugation of its cytosolic form LC3-I to phosphatidyl-ethanolamine. This protein is commonly used as an autophagic marker because of its association to the autophagic compartments throughout the entire process. As these compartments possess a double membrane, the LC3-II protein present in the inner membrane will be degraded once the autophagosomes fuse with the lysosomes. The use of protease inhibitors abolishes this part of the process and allows to visualize the total LC3-II mobilized

proteins, but also to estimate the rate of autophagic turnover by comparing the conditions with and without protease inhibitors (Figure 3A and 3D). Using the same parameters of incubation time and activation described above, we quantified the LC3-II protein by measuring the density of the bands relative to β-Actin, serving as the protein loading control (Figure 3B and 3E). As expected we had a high accumulation of autophagic membranes in physiologically and pharmacologically activated conditions both in T (antiCD3/CD28 or P/I) and B cells (LPS or P/I) in comparison to the untreated cells. However, we did not see variations when comparing with conditions incubated with graphene. Also, the evaluation of the autophagic flux did not evidence statistically significant differences (Figure 3C and 3F). Thus, it seems that FLG has no major impact on this cellular process. Autophagy was shown to be a complex and fine-tuned process in lymphocytes. In B cells the importance of this mechanism appears to vary depending on their stage of differentiation and the immunological compartment they are localized in, but autophagy is mostly required for the survival of long-lived antibody-secreting B derived plasma cells.[26,27] In the case of T cells, autophagy is essential for the formation of memory CD8+ T cells, while for memory CD4+ T cells, it is required for their survival. Overall, it is rather reassuring that FLG does neither decrease nor increase autophagy. This is in contrast with other GBMs such as carbon nanotubes or GO, that have been shown to rather block the autophagic flux in RAW macrophages and peritoneal macrophages, respectively.[15,27] A very recent study, demonstrated that FLG at low doses could trigger autophagy in an ER-stress dependent manner and act as a protective mechanism in macrophages.[28] In our case, it is the first time that the impact of FLG on autophagy is focused on the major players of the adaptive immune response and as such, it could be interesting to study its impact on memory immune responses as well. Indeed, in *in vivo* settings, it is possible that this material might remain for longer times in the body, possibly triggering a response that could also impact autophagic functions. In an *in vivo* study by Sasidharan *et al.*, it was observed in fact, the presence of pristine and functionalized graphene

aggregates in some organs (lung, liver, and spleen) of mice, up to 90 days post-injection of the material.[29]

3.4. Evaluation of intracellular stress in lymphocytes incubated with FLG

Despite the fact that we noticed no particular changes in the autophagic turnover, we could not rule out the possibility of early signs of cellular stress. For this purpose, we evaluated the mitochondria load in the lymphocytes, their functional state (Figure 4), and the production of ROS (Figure 5). By incubating the cells with two dyes, mitotracker green (MT-Green) and mitotracker deep red (MT-DeepRed) and using flow cytometry, we were able to distinguish three cell populations (Figure 4A). Since MT-Green stains all mitochondrial membranes, it allows to evaluate the mitochondrial load, while MT-DeepRed, being sensitive to mitochondrial potential, is useful to establish the respiratory status of these organelles. As in all our experiments the lymphocytes were incubated for 24 h in the indicated conditions (Figure 4B). We observed as expected different distributions of the three populations depending on the cell type, reflecting the differences in metabolism between T and B lymphocytes. In both we saw an increased percentage of cells with a high mitochondrial content (MT-Green high and MT-DeepRed high) associated with a decrease in cells with damaged mitochondria (MT-Green high and MT-DeepRed low) when the lymphocytes were activated (Figure 4A). The presence of FLG, in the activated conditions, did not significantly alter these parameters even though it appeared a slight increase of damaged mitochondria in LPS activated B cells in the presence of the highest concentration of FLG (100 µg mL^{-1}, Figure 4B). A minor diminution in T and B cells with a high mitochondria load, when incubated with 100 µg/mL FLG alone, is also observable. The assessment of ROS production was also done by flowcytometry. We used MitoSOX to detect the production of superoxide, the major mitochondrial ROS (Figure 5A). In T lymphocytes, superoxide was in average higher than in B cells, but the presence of graphene did not remarkably alter the generation of superoxide (Figure 5B). In B lymphocytes, however, we could measure a small increase of

ROS in the conditions incubated with 100 µg mL^{-1} FLG. The overall conclusion to these observations is that at 24 h there are no significant metabolic variations as demonstrated in mitochondrial load and function. On the other hand, we cannot completely rule out that at longer incubation times, this would not change as some results point out signs of cellular stress, which could potentially have an impact on autophagic functions as well. In fact, a comparative study between FLG and GO impact on metabolic function of a keratinocyte cell line, led to the conclusion that FLG is able to induce a significant increase in ROS production after 7 days of incubation with the material.[30]

3.5. Study of the interaction of FLG with the lymphocyte cell membranes and autophagic compartments

In addition to the previous observations, we wanted to better understand the nature of the interaction of FLG with the lymphocytes. This could indeed be evaluated by immunofluorescence using confocal microscopy. In order to visualize the FLG, we functionalized this material with quantum dots (QD). After analysis of the images we noticed that the FLG-QD (pink) were in close vicinity to the B cell membrane (MHC-II staining, red) but also the T cell membrane (TCRb staining, red) (Figure 6A and 6B). The FLG was also observed by transmission as black spots that overlap with the pink staining (see Trans-Merge panels). However, we did not see any co-localization with the membranes. Even though we did not study the nature of this interaction in detail, we can hypothesize that it does not induce membrane damages, since we could neither observe them by carefully analyzing the Z-stacking of the confocal images (see Supplementary Figure S2 and S3 and Video S2 and S3), nor did we see any specific toxicity effect, as demonstrated in previous experiments (Figure 2-5). Nevertheless, this does not exclude a lipid-graphene interaction. Indeed, graphene sheets have been shown to interact with membrane lipids in various manners, leading possibly to lipid extraction, which appears to be influenced by the polarity and curvature of the material.[31,32] This aspect requires further investigation in order to understand exactly how

FLG interacts with the lymphocyte membrane and if this proximity is indeed entirely harmless. But given our results on viability, autophagic activity and oxidative stress, so far there is no indication that the physical interaction with the lymphocytes membranes induces any damage.

We were also interested in investigating whether the FLG could be seen interacting or even inside the autophagic membranes. For this purpose, we did a LC3 staining (green) (Figure 6A and 6B). As LC3 proteins are both cytosolic (LC3-I) as well as membrane-bound (LC3-II), the presence of autophagosomes is demonstrated by the formation of dots. Judging from the confocal images and their 3D reconstruction, we saw neither the presence of FLG inside the cells nor in co-localization with the LC3 dots (see Supplementary Figure S2 and S3 and Video S2 and S3). These observations were mostly qualitative and not quantifiable *per se*, but they can explain why we did not see any difference when quantifying the autophagic activity by Western blot (Figure 3). It is also important to mention that these cells have a very small cytoplasm, which could limit the penetration of the material and confer a certain protection. So far, most observations have been focusing on macrophages and in these cells FLG could be easily seen in their cytoplasm, associated to an increased autophagic activity and oxidative stress.[28] This seems to indicate that FLG influences mostly cellular functions of phagocytic cells while the lymphocytes are spared.

4. Conclusion

This study has allowed us to reach a better understanding of primary lymphocyte function in the presence of few layer graphene. By using FLG that can be easily dispersed in cell culture media, we were able to show that this material does not lead to significant death of the lymphocytes. Even though it appears to exert some activation effects in B cells, these effects seem mild and they do not occur in T cells. We also analyzed the general autophagic activity, which is important to maintain normal cellular functions, but we did not see again any

changes. This is also in agreement with the observations, made by confocal microscopy, showing an interaction with the cell membrane whereas no material was visualized inside the cells. On the other hand, we could not increase the FLG concentration above 100 µg/mL since we had to take into account the limit in dispersibility of the material. Too high concentrations would have led to the formation of big aggregates that would have not been internalized by lymphocytes that are small non-phagocytic cells.

Considering all our data, FLG appears to be overall safe on the lymphocytes, which is a first step in favor of *in vivo* studies. In this case, it would be of great interest to further investigate the impact of FLG on lymphocyte autophagy and function on the long-term but also its influence on the interaction of lymphocytes with other immune cells in order to have a throrough overview of the impact of our material on immune basic functions. A follow-up of this work in tumor models might also allow us to better link the data obtained in this study to the results from Russier *et al.* and explain the observed discrepancies in terms of B cell activation and if this difference can be observed in *in vivo* settings. However, the specificity of FLG to induce cell death in monocytes while spearing other immune cells and the mild impact seen on lymphocytes in our conditions, are in favor of further pursuing the studies on FLG in biological systems. FLG may indeed be an interesting tool to be used in the future, in combined therapies to treat cancers such as acute myeloid leukaemia or even other monocyte associated disorders. Thus, investigating the safety of this material and its impact on different cells and cell functions such as autophagy is a key step towards this goal.

Conflicts of interest

All the authors do not declare any conflicts of interest with this work.

Acknowledgements

The authors gratefully acknowledge the financial support from the EU GRAPHENE Flagship project (no. 696656 and no. 785219), from the Agence Nationale de la Recherche (ANR) through the LabEx project Chemistry of Complex Systems (ANR-10-LABX-0026_CSC), and through the program "Investissements d'Avenir" (ANR-11-EQPX-022). This work was partly supported by the Centre National de la Recherche Scientifique (CNRS), the International Center for Frontier Research in Chemistry (icFRC) and the Spanish Ministerio de Economía y Competitividad (project CTQ2014-53600-R).

Electronic supplementary information (ESI) available: See DOI: See 10.1039/c9nr00846b

References

1 X. Huang, Z. Yin, S. Wu, X. Qi, Q. He, Q. Zhang, Q. Yan, F. Boey and H. Zhang, *Small*, 2011, **7**, 1876–1902.

2 S. Gurunathan and J.-H. Kim, *Int. J. Nanomedicine*, 2016, **11**, 1927-1945.

3 A. K. Geim and K. S. Novoselov, *Nat. Mater.*, 2007, **6**, 183–191.

4 S. M. A. Cruz, A. F. Girão, G. Conçalves and P. A. A. P. Marques, *Sensors*, 2016, **16**, 137.

5 V. C. Sanchez, A. Jachak, R. H. Hurt and A. B. Kane, *Chem. Res. Toxicol.*, 2012, **25**, 15–34.

6 S. Sharifi, S. Behzadi, S. Laurent, M. Laird Forrest, P. Stroeve and M. Mahmoudi, *Chem. Soc. Rev.*, 2012, **41**, 2323–2343.

7 A. Madni, S. Noreen, I. Maqbool, F. Rehman, A. Batool, P. M. Kashif, M. Rehman, N. Tahir and M. I. Khan, *J. Drug Target.*, 2018, **26**, 858–883.

8 G. Reina, J. M. González-Domínguez, A. Criado, E. Vázquez, A. Bianco and M. Prato, *Chem. Soc. Rev.*, 2017, **46**, 4400–4416.

9 G. Lalwani, M. D'Agati, A. M. Khan and B. Sitharaman, *Adv. Drug Deliv. Rev.*, 2016, **105**, 109–144.

10 N. Mizushima, *Cold Spring Harb. Symp. Quant. Biol.*, 2011, **76**, 397–402.

11 G. Mariño, M. Niso-Santano, E. H. Baehrecke and G. Kroemer, *Nat. Rev. Mol. Cell Biol.*, 2014, **15**, 81–94.

12 W. Zheng, M. Wei, S. Li and W. Le, *Nanomedicine*, 2016, **11**, 1417–1430.

13 G.-Y. Chen, H.-J. Yang, C.-H. Lu, Y.-C. Chao, S.-M. Hwang, C.-L. Chen, K.-W. Lo, L.-Y. Sung, W.-Y. Luo, H.-Y. Tuan and Y.-C. Hu, *Biomaterials*, 2012, **33**, 6559–6569.

14 M. Orecna, S. H. De Paoli, O. Janouskova, T. Z. Tegegn, M. Filipova, J. E. Bonevich, K. Holada and J. Simak, *Nanomedicine Nanotechnology, Biol. Med.*, 2014, **10**, e939–

e948.

15 V. Cohignac, M. J. Landry, A. Ridoux, M. Pinault, B. Annangi, A. Gerdil, N. Herlin-Boime, M. Mayne, M. Haruta, P. Codogno, J. Boczkowski, J.-C. Pairon and S. Lanone, *Autophagy*, 2018, **14**, 1323–1334.

16 V. Deretic, T. Saitoh and S. Akira, *Nat. Rev. Immunol.*, 2013, **13**, 722–737.

17 L. Muzi, F. Mouchet, S. Cadarsi, I. Janowska, J. Russier, C. Ménard-Moyon, G. Risuleo, B. Soula, A.-M. Galibert, E. Flahaut, E. Pinelli, L. Gauthier and A. Bianco, *2D Mater.*, 2016, **3**, 025009.

18 M. Pelin, L. Fusco, V. León, C. Martín, A. Criado, S. Sosa, E. Vázquez, A. Tubaro and M. Prato, *Sci. Rep.*, 2017, **7**, 40572.

19 J. Russier, V. León, M. Orecchioni, E. Hirata, P. Virdis, C. Fozza, F. Sgarrella, G. Cuniberti, M. Prato, E. Vázquez, A. Bianco and L. G. Delogu, *Angew. Chemie Int. Ed.*, 2017, **56**, 3014–3019.

20 V. León, J. M. González-Domínguez, J. L. G. Fierro, M. Prato and E. Vázquez, *Nanoscale*, 2016, **8**, 14548–14555.

21 J. M. González-Domínguez, V. León, M. I. Lucío, M. Prato and E. Vázquez, *Nat. Protoc.*, 2018, **13**, 495–506.

22 X. Wang, C. Xie, J. Zhong, X. Liang and W. Xiang, *J. Alloys Compd.*, 2015, **648**, 127–133.

23 G. Reina, A. Ruiz, D. Murera, Y. Nishina and A. Bianco, *ACS Appl. Mater. Interfaces*, 2019, **11**, 7695–7702.

24 M. Orecchioni, D. Bedognetti, L. Newman, C. Fuoco, F. Spada, W. Hendrickx, F. M. Marincola, F. Sgarrella, A. F. Rodrigues, C. Ménard-Moyon, G. Cesareni, K. Kostarelos, A. Bianco and L. G. Delogu, *Nat. Commun.*, 2017, **8**, 1109.

25 W. Liu, C. Sun, C. Liao, L. Cui, H. Li, G. Qu, W. Yu, N. Song, Y. Cui, Z. Wang, W. Xie, H. Chen and Q. Zhou, *J. Agric. Food Chem.*, 2016, **64**, 5909–5918.

26 H. Sandoval, S. Kodali and J. Wang, *Mitochondrion*, 2018, **41**, 58–65.

27 B. Wan, Z.-X. Wang, Q.-Y. Lv, P.-X. Dong, L.-X. Zhao, Y. Yang and L.-H. Guo, *Toxicol. Lett.*, 2013, **221**, 118–127.

28 L. Di Cristo, S. Mc Carthy, K. Paton, D. Movia and A. Prina-Mello, *2D Mater.*, 2018, **5**, 045033.

29 A. Sasidharan, S. Swaroop, C. K. Koduri, C. M. Girish, P. Chandran, L. S. Panchakarla, V. H. Somasundaram, G. S. Gowd, S. Nair and M. Koyakutty, *Carbon N. Y.*, 2015, **95**, 511–524.

30 J. Frontiñán-Rubio, M. V. Gómez, C. Martín, J. M. González-Domínguez, M. Durán-Prado and E. Vázquez, *Nanoscale*, 2018, **10**, 11604–11615.

31 B. Luan, S. Zhou, D. Wang and R. Zhou, *ACS Nano*, 2017, **11**, 12615–12623.

32 Y. Roiter, M. Ornatska, A. R. Rammohan, J. Balakrishnan, D. R. Heine and S. Minko, *Nano Lett.*, 2008, **8**, 941–944.

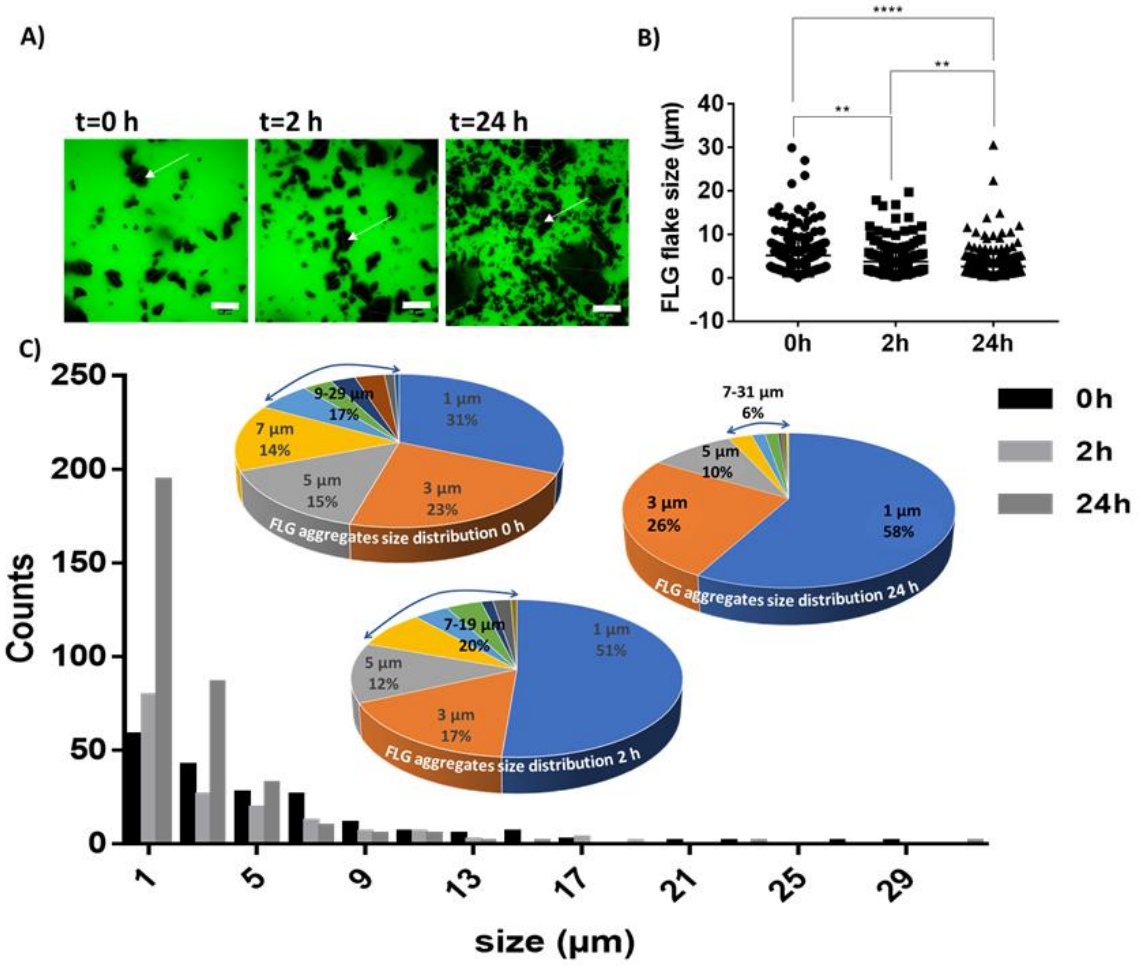

Figure 1: Study of FLG aggregates dispersion in culture media. A) Representative confocal images taken at 0 h, 2 h and 24 h after the dispersion of FLG in FBS supplemented RPMI medium at 0.1 mg mL^{-1} and in presence of fluorescein (in green). The white arrows indicate the FLG aggregates at the bottom of the vial. The observations were made with a 100× objective and the indicated scale is of 20 µm. B) Graph representing the size distribution of the FLG aggregates measured from the confocal images at the bottom of the vial at 0 h, 2 h and 24 h. C) Graph representing the aggregates counted according to their size and the size distribution in % according to the total number of aggregates counted for each time point. Three images per time point were taken for measuring and counting the aggregates. **p<0.007; ****p<0.00005 (One-way ANOVA, Tukey test).

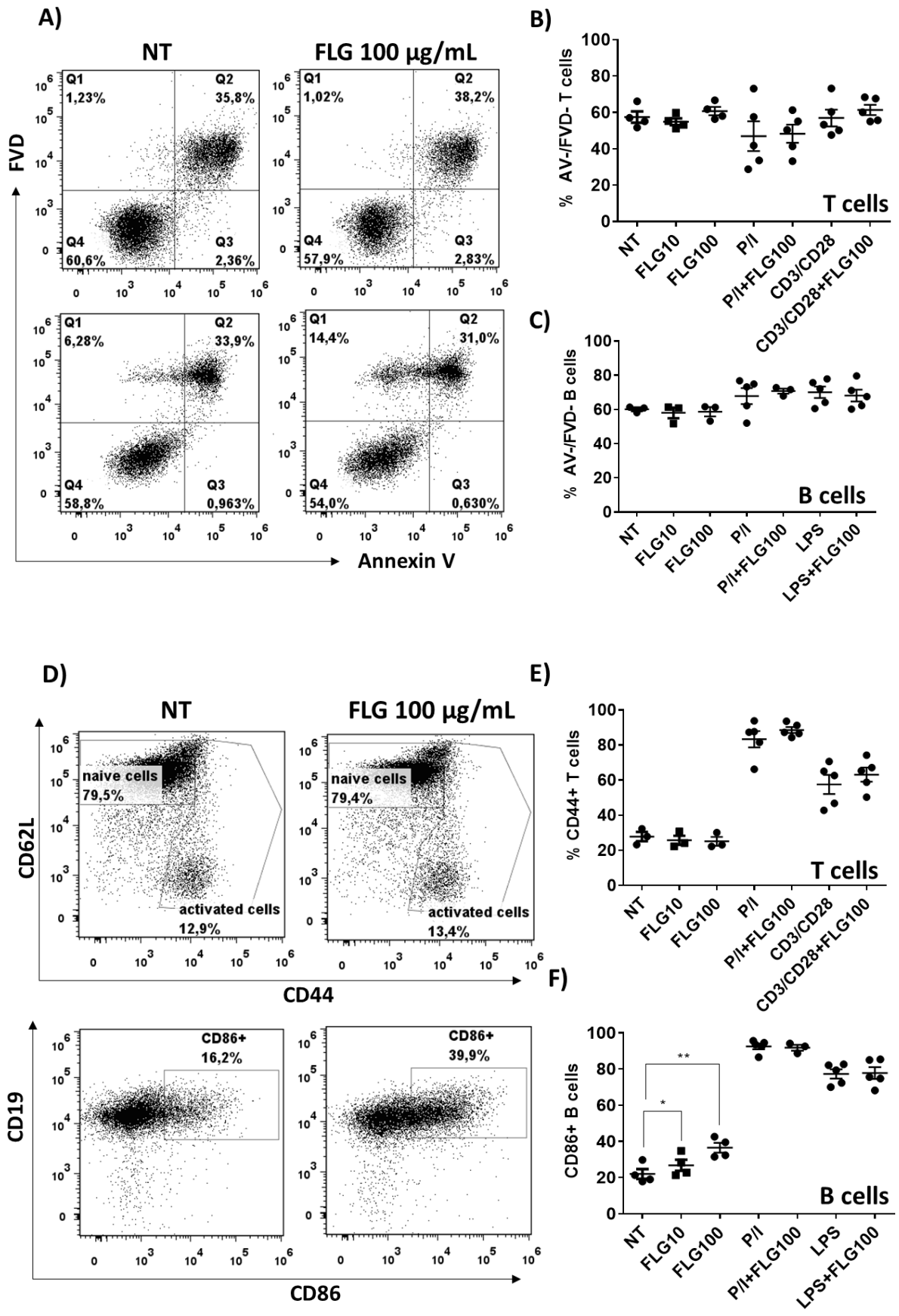

Figure 2: Impact of FLG on lymphocyte function. A) Representative flow cytometry dot plots illustrating the viability staining of T and B lymphocytes with FVD and Annexin V after

24 h incubation. The two left panels show the staining of the cells that were not treated (NT) and the right panels the cells that were incubated with FLG at a concentration of 100 µg mL^{-1}. B) Relative percentages of T lymphocytes with a negative staining for annexin V (AV-) and FVD (FVD-) after 24 h incubation in the indicated conditions. Each point represents an independent experiment. (P/I= phorbol 12- myristate 13-acetate and ionomycin, CD3/CD28 = anti-CD3+anti-CD28, FLG100 = 100 µg mL^{-1} FLG). C) Relative percentages of B lymphocytes with a negative staining for Annexin V (AV-) and FVD (FVD-) after 24 h incubation in the indicated conditions. Each point represents an independent experiment. (LPS= lipopolysaccharide). D) Representative flow cytometry dot plots showing the expression of T (top) and B cell (bottom) activation markers CD62L/CD44 and CD86 respectively, after 24 h activation. E) Relative percentages of activated (=CD44+) T cells for the indicated conditions after 24 h incubation. F) Relative percentages of activated (=CD86+) B cells for the indicated conditions after 24 h incubation. n=3-5, *P< 0.05; **P <0.01 (One-way ANOVA, Tukey test).

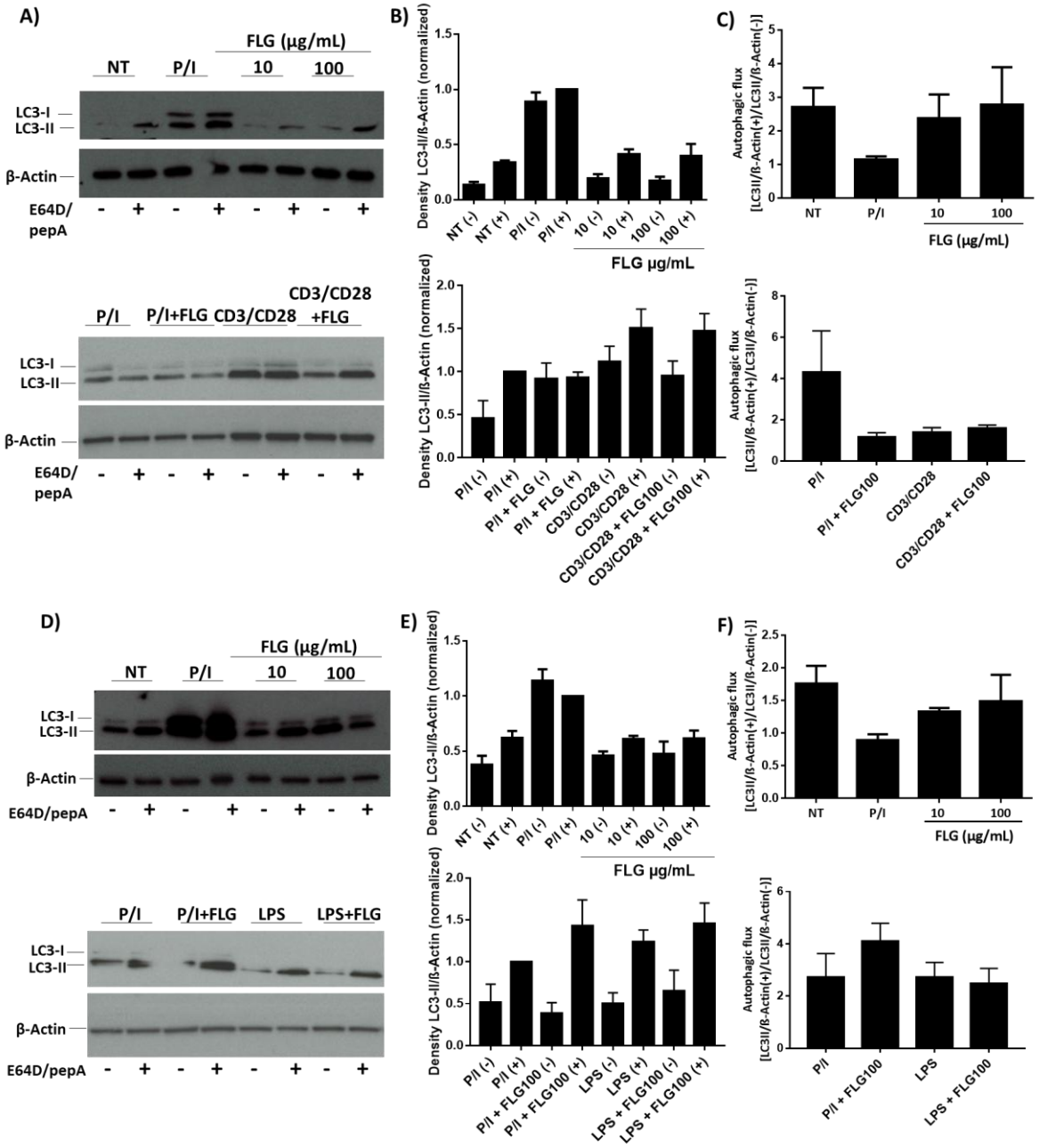

Figure 3: Evaluation of FLG capacity to modulate the autophagic activity in lymphocytes. A) Representative Western-blots of the LC3 proteins in T cells incubated for 24 h with the indicated conditions and treated 4 h prior the end of the culture with protease inhibitors [E64D/pepstatin A (pepA)]. Expression of β-Actin was used as an internal protein loading control. B) Relative quantification of the density of LC3-II normalized to β-Actin (ratio LC3-II/β-ActP/Iin) and to the condition P/I (+). C) Evaluation of the autophagic flux by representing the ratio between the conditions with (+) and without (+) E64D/pepA, n=3-4. D) Representative Western-blots of the LC3 proteins in B cells incubated for 24 h with the

indicated conditions and treated 4 h prior the end of the culture with protease inhibitors E64D and pepA. Expression of b-Actin was used as an internal protein loading control. E) Relative quantification of the density of LC3-II normalized to b-Actin (ratio LC3-II/β-Actin) and to the condition P/I (+). F) Evaluation of the autophagic flux by representing the ratio between the conditions with (+) and without (+) E64D/pepA, n=3. P>0.05 (One-way ANOVA, Tukey test)

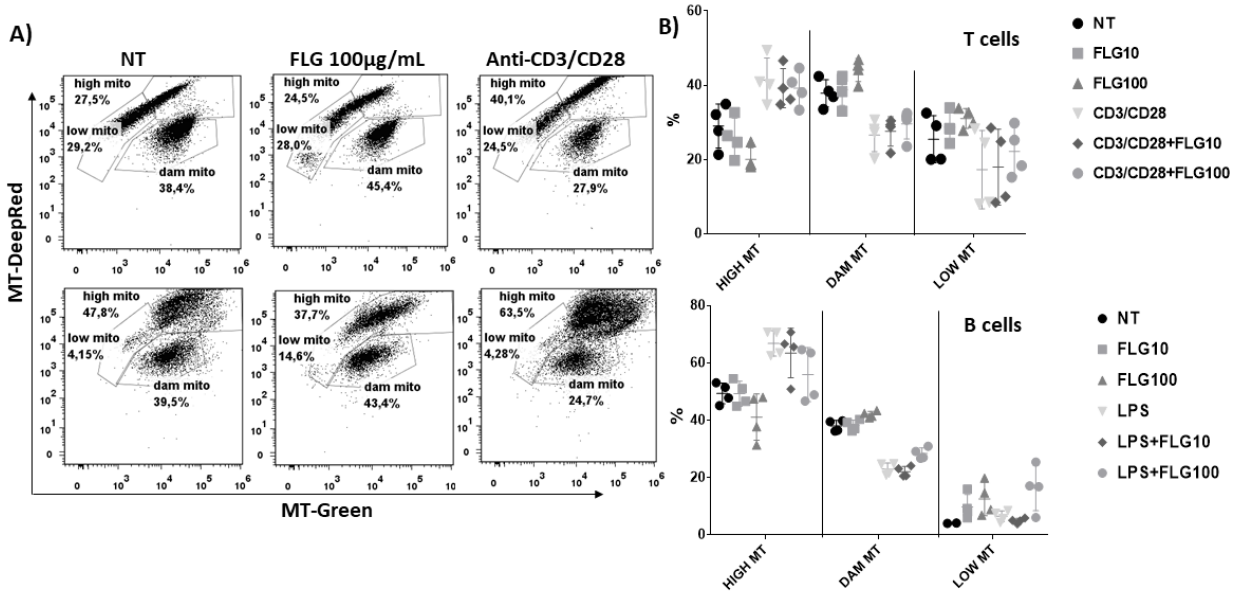

Figure 4: Impact of graphene-lymphocyte interaction on mitochondrial load. A) Representative flow cytometry dot plots of T and B lymphocytes after MitoTracker deep red (MT-DeepRed) and MitoTracker green (MT-Green) staining. Three cell populations can be distinguished: cells with a high mitochondrial content (HIGH MT), cells with damaged mitochondria (DAM MT) and cells with a low mitochondrial content (LOW MT). B) Relative percentages of the mitochondrial content in T and B lymphocytes in the indicated conditions, n=4. P>0.05 (One-way ANOVA, Tukey test)

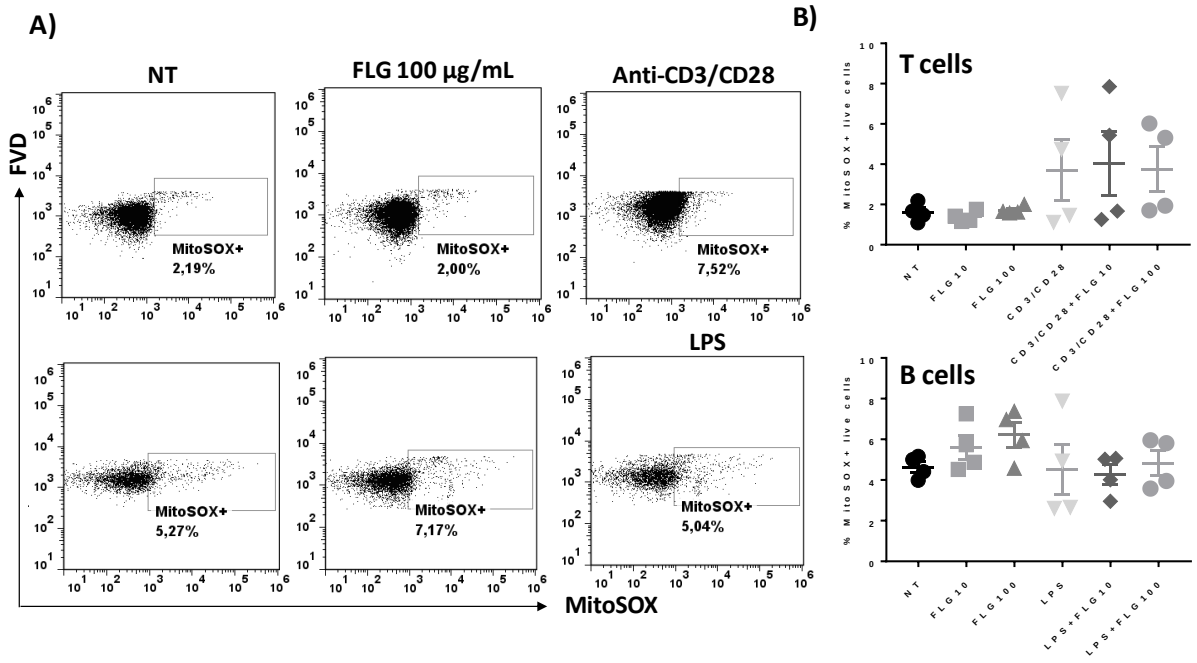

Figure 5: Modulation of ROS production in B and T cells in the presence of FLG. A) Representative flow cytometry dot plots of T and B lymphocytes after incubation with the superoxide marker (MitoSOX) and the fixable viability dye (FVD). B) Relative percentages of MitoSOX positive live T and B lymphocytes for the indicated conditions, n=4. P>0.05 (One-way ANOVA, Tukey test)

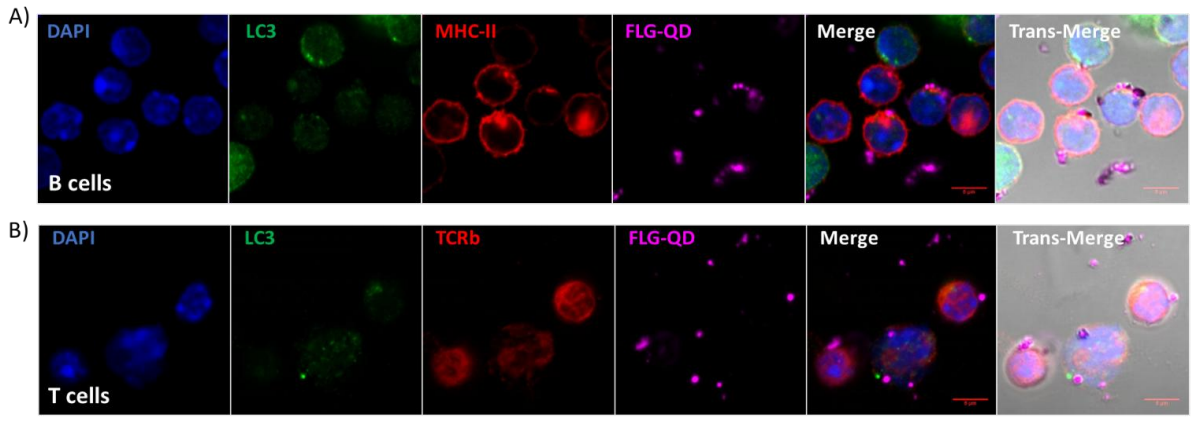

Figure 6: Study of the interaction of FLG with lymphocyte membranes and autophagic compartments. A) Representative confocal images of B lymphocytes after 24 h incubation with 10 µg mL^{-1} FLG-QD. The nucleus is stained with DAPI (blue), the autophagosomes with an anti-LC3 antibody (green) and the membranes with an anti-MHC-II antibody (red). The three staining are shown in a merged image with and without the transmission. B) Representative confocal images of T lymphocytes after 24 h incubation with 10 µg mL^{-1} FLG-QD (pink). The nucleus is stained with DAPI (blue), the autophagosomes with an anti-LC3 antibody (green) and the membranes with an anti-TCRb antibody (red). The three staining are shown in a merged image with and without the transmission image.